Composites Part B 261 (2023) 110788

Contents lists available at ScienceDirect

Composites Part B

journal homepage: www.elsevier.com/locate/compositesb

A comprehensive experimental investigation of the rate-dependent interlaminar delamination behaviour of CFRP composites

Yanhong Chen [a], Kai Liu [a], Ziwen Xu [a,*], Huifang Liu [a], Maria Lißner [a,b,c], Borja Erice [a,d,e], Nik Petrinic [a]

[a] Department of Engineering Science, University of Oxford, Oxford, OX1 3PJ, United Kingdom
[b] Dresden Centre for Intelligent Materials, Dresden University of Technology, Dresden, 01069, Germany
[c] Institute of Lightweight Engineering & Polymer Technology, Dresden University of Technology, Dresden, 01307, Germany
[d] Mondragon Unibertsitatea, Faculty of Engineering, Department of Mechanics and Industrial Production, Loramendi 4, Arrasate-Mondragon 20500, Gipuzkoa, Spain
[e] IKERBASQUE, Basque Foundation for Science, Bilbao, Spain

ARTICLE INFO

Handling Editor: Ole Thomsen

Keywords:
Interlaminar fracture toughness
Rate-dependent delamination
Critical energy release rate
CFRP composites

ABSTRACT

The paper presents a systematic experimental study of the interlaminar delamination behaviour of a carbon composite subjected to Mode I, Mode II and Mixed-mode delamination at both quasi-static (QS) and high-rate (HR) conditions, which were conducted on a screw-driven test machine and in-house Hopkinson bar systems, respectively. A methodology integrating digital image correlation and the compliance-based beam theory was employed to circumvent the challenges in measuring the loads at HR tests and maintain good consistency during the data analysis of all delamination tests. The results demonstrated a positive rate-dependent delamination behaviour, with the HR Mode I, Mode II and Mixed-mode fracture toughness properties being 1.56, 1.66 and 1.60 times their QS counterparts, respectively. The cause of such a dependency was revealed following a detailed fractographic analysis, which highlighted that the observed dependency was associated with the transition of the predominant failure mechanisms in the QS and HR conditions.

1. Introduction

Compared to metallic counterparts, fibre-reinforced polymer (FRP) composites can offer various benefits including high specific strength and stiffness. Owing to their high structural efficiency, FRP composites are extensively employed in the aerospace industry to manufacture high-performance components, such as aircraft fuselage, wings and engine blades [1]. However, FRP composites are also known for their susceptibility to interlaminar delamination, which is one of the most detrimental failure modes that may cause significant degradation of structural integrity or even catastrophic failure. Therefore, obtaining a clear understanding of the resistance to interlaminar delamination (also known as interlaminar fracture toughness or critical energy release rate (ERR), G_c) by performing fracture toughness characterisation testing is of paramount importance for developing load-bearing structures based on FRP composites.

The characterisation of interlaminar fracture toughness of FRP composites is an intricate experimental problem as interlaminar delamination is a complex failure phenomenon commonly involving Mode I (opening) separation, Mode II (shear) separation and Mixed-mode I/II separation i.e., a combination of Mode I and Mode II delamination. This problem can be further complicated by the rate sensitivity of FRP composites. Over the past several decades, considerable efforts have been devoted to characterising interlaminar fracture toughness properties of various FRP composites subjected to Mode I [2–13], Mode II [14–22], and Mixed-mode I/II loading conditions [18,23,24]. The published studies demonstrated that the interlaminar fracture toughness properties of FRP materials can be insensitive to the loading rate or may exhibit positive or negative rate dependency on the loading rate. After reviewing much of the published work on this topic, Jacob et al. [25] highlighted a lack of consensus on the rate dependency of the fracture toughness properties of composite materials, which was associated with the rate-sensitivity of polymer matrix and the presence of failure mode transition in the fracture process zone (FPZ) at different loading rates. In the reviews recently conducted by May and colleagues [26,27], the presence of inconsistent findings on the rate-dependent interlaminar fracture behaviour of composites was attributed to the lack of established test methods for high-rate (HR) fracture testing. Indeed, various challenges arise in HR fracture toughness testing of composites, which is

* Corresponding author.
E-mail address: ziwen.xu@eng.ox.ac.uk (Z. Xu).

https://doi.org/10.1016/j.compositesb.2023.110788
Received 22 September 2022; Received in revised form 7 April 2023; Accepted 3 May 2023
Available online 11 May 2023

Nomenclature

Symbols	*Description*
α	Power of the power law criterion
δ	Opening displacement or beam deflection (mm)
η	Power of the Benzeggagh-Kenane criterion
a	Crack length (mm)
a_0	Initial crack length (mm)
a_e	Effective crack length (mm)
Δa	Crack length increment (mm)
b	Specimen width (mm)
c	Wave velocity (mm/s)
C	Compliance (mm/N)
C_0	Initial compliance (mm/N)
E_1	Longitudinal elastic modulus (MPa)
E_3	Transverse elastic modulus (MPa)
E_f	Flexural modulus (MPa)
F	Opening or bending force (N)
G_{13}	Shear modulus (MPa)
G_c	Fracture toughness (N/mm)
G_I	Mode I strain energy release rate (N/mm)
G_{Ic}	Mode I fracture toughness (N/mm)
G_{II}	Mode II strain energy release rate (N/mm)
G_{IIc}	Mode II fracture toughness (N/mm)
$G_{I/IIc}$	Mixed-mode I/II fracture toughness (N/mm)
G_T	Total strain energy release rate (N/mm)
h	Half specimen thickness (mm)
L	Characteristic specimen length (mm)
L_s	Total specimen length (mm)
t_C	Support reaction time (s)
t_R	Reference time (s)
t_T	Characteristic time (s)

primarily due to the difficulty in accurately obtaining the necessary data (particularly the load history) for calculating the fracture toughness. Although various experimental approaches have been proposed to address the HR fracture toughness characterisation of composites, they come with both advantages and limitations from the perspectives of specimen geometry, test setup and data acquisition [26,27].

To address the challenges in HR fracture toughness testing of composites, a few recent studies focused on the development of methodologies capable of circumventing the measurement of the load data in HR tests [13,28–30]. Isakov et al. [13] proposed a combined experimental-analytical approach to obtain the HR Mode I fracture toughness of a carbon fibre-reinforced polymer (CFRP) composite. Based on a loading wedge that was geometrically shaped with a round head followed by a constant cross-section, a modified wedge-loaded double cantilever beam (WDCB) was introduced to delaminate the specimen of testing, and the deformation history of the specimen adherents was

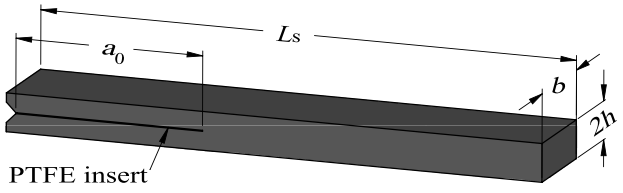

(a) WDCB: L_s = 142, a_0 = 50, b = 20 and h = 2.075.

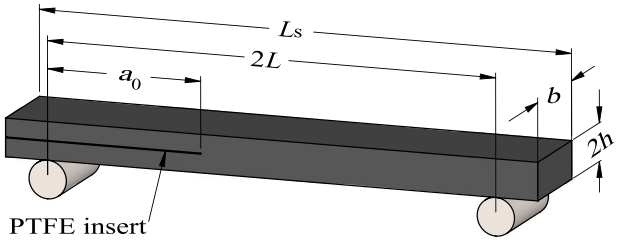

(b) ENF: L_s = 150, L = 65, a_0 = 45, b = 20 and h = 2.075.

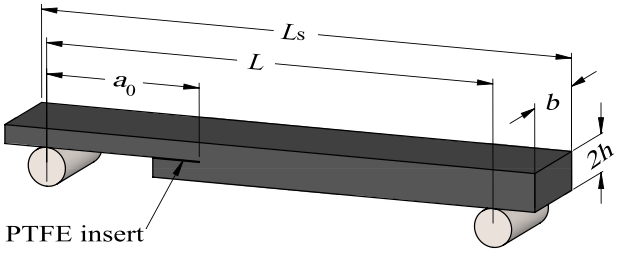

(c) SLB: L_s = 150, L = 130, a_0 = 45, b = 20 and h = 2.075.

Fig. 1. WDCB, ENF and SLB specimen geometry and dimensions (mm).

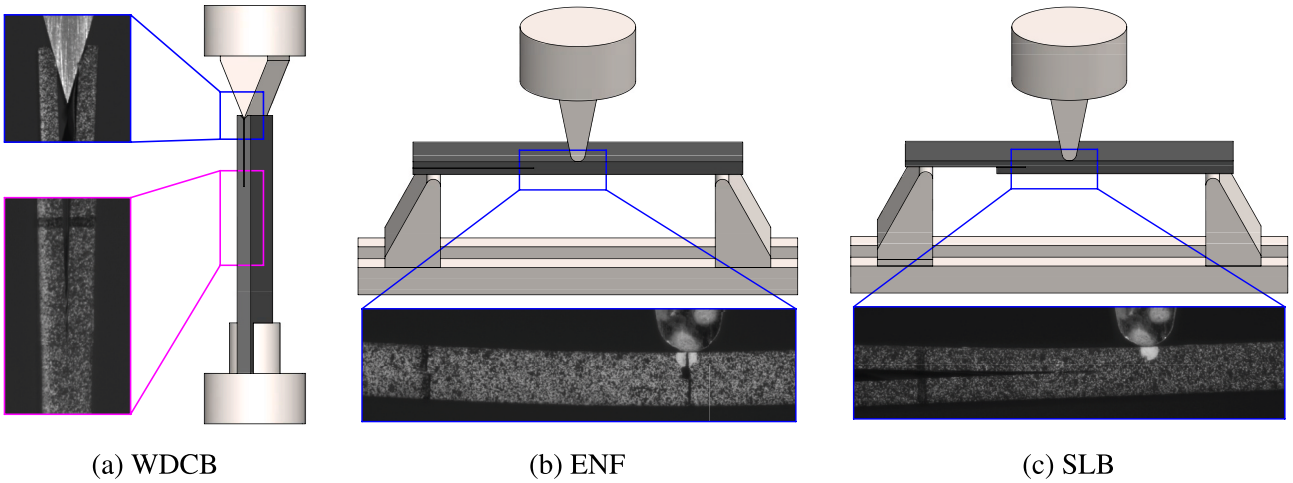

Fig. 2. WDCB, ENF and SLB setups for QS (1 mm/min) fracture toughness testing.

tracked using a high-resolution camera. By fitting the beam theory to the optically tracked results, the HR fracture toughness was computed without any force data from the experiment. Liu et al. [28,29] developed a hybrid numerical-experimental approach for the HR Mode I fracture toughness characterisation of CFRP composites. In their work, a Hopkinson bar system containing two identical incident bars was employed to perform the HR Mode I tests. Combining the opening displacement history obtained using a high-speed camera and the crack length data derived using a wire-based electric gauge, a finite element (FE) simulation with user-defined cohesive elements was conducted to predict the opening load and subsequently to calculate the fracture toughness based on an energy balance technique, avoiding the need for experimentally measuring the opening load. Recently, Ponnusami et al. [30] investigated the dynamic Mode-I fracture properties of CFRP composites by using an integrated numerical-experimental strategy. The experimental part involved testing WDCB specimens using a split Hopkinson pressure bar (SHPB) to obtain the strain-displacement response, the opening displacement history and the crack length data. Following the experimental tests, numerical simulations with different inputs for the fracture toughness property of the cohesive elements were conducted. Without deriving the force history of the experiment, the Mode I fracture toughness property was identified by fitting the numerical results against the experimental data. Here, it should be kept in mind that the outline methodologies were developed for determining the HR Mode I fracture toughness of CFRP composites. Their applicability to the fracture toughness characterisation of HR Mode II and Mixed-mode delamination still needs to be evaluated and understood.

The literature review above suggests further need for investigating the rate-dependent interlaminar delamination behaviour of FRP composites. Therefore, the present research was aimed at deepening our understanding of this research topic by conducting Mode I, Mode II and Mixed-mode I/II fracture testing of a commercial CFRP composite at both QS and HR loading conditions. Three strategic measures were taken to maximise the outcome. First, all delamination tests of the present research were undertaken in a single experimental programme and performed by the same researchers, attempting to minimise the potential discrepancies associated with different testing programmes and operators. Second, an experimental methodology integrating digital image correlation (DIC) and the compliance-based beam method (CBBM), which was developed by Liβner et al. [31,32] for adhesively bonded structures, was adapted to the present experimental programme. The integrated DIC-CBBM methodology was proposed to circumvent the challenge of measuring the load of HR fracture testing and was proven to be valid for both QS and HR testing of different delamination modes. The primary purpose of adapting this methodology to the present research was to avoid the possible inconsistencies that originated from using different approaches for different types of fracture tests. Third, a detailed fractographic analysis based on 3D optical metrology and scanning electron microscopy (SEM) was conducted as supplementary material to validate the proposed experimental study, as well as to correlate the rate-dependent delamination behaviour of the CFRP composite with the physical mechanisms that occurred at the delamination interface. The remainder of this paper is structured by describing the experimental methods in the second section, discussing the results in the third section and lastly concluding the findings and contributions of the present research.

2. Experimental methods

2.1. Material & specimen preparation

The material investigated in the present research was based on a Hexcel toughened epoxy prepreg, which is a high-performance carbon fibre-reinforced epoxy matrix system developed for composite aircraft structures. All specimens were cut from a unidirectional (UD) laminated panel fabricated from 16 layers of the prepreg aligned in the 0° direction. Following the recommended temperature profile [33], the panel was cured at dwelling temperatures of 110 °C for 60 min and 180 °C for 120 min, resulting in an average panel thickness of 4.15 mm. A 13 μm polytetrafluoroethylene (PTFE) film was inserted between the 8th and 9th plies to form a pre-crack. WDCB, ENF and single leg bending (SLB) specimens were used for the Mode I, Mode II and Mixed-mode I/II fracture toughness testing, respectively. As illustrated in Fig. 1, all three types of specimens had a total width of 20 mm and an overall thickness of 4.15 mm. The WDCB specimens had a 50 mm pre-crack along with a small notch machined at the pre-crack end to ensure that the sharp tip of the loading wedge can be accurately positioned in the middle plane of the beam. The initial crack lengths of the ENF and SLB specimens were the same and equal to 45 mm. For all three cases, one side of each specimen was sprayed into a matt white background with black speckles on the top to create a fine DIC pattern to facilitate the observation of crack propagation during testing and allow for post-test DIC analysis of the recorded video.

2.2. Experimental procedures

All three types of fracture toughness characterisation tests at QS loading rates were conducted on a screw-driven test machine (Zwick-Roell Z050) at a displacement rate of 1 mm/min. High-resolution cameras were employed to record videos for post-test DIC analysis at a recording rate of 2 frames per second (fps) and with a resolution of 2456 × 900 pixels, as illustrated in Fig. 2. For WDCB testing, the specimens were aligned vertically with their lower end supported by a notched cylindrical holder which was further fixed to the platen of the machine, as indicated in Fig. 2a. The loading wedge, which has a sharp tip with an angle of 30°, was positioned near the specimen notch and moved downward by the upper crosshead of the machine to crack the specimen. For ENF and SLB testing, the specimens were horizontally rested on two steel supports and transversely loaded by the loading wedge connected to the upper crosshead, as shown in Fig. 2b and c, respectively. Both the loading wedge and support blocks were manufactured with a cylindrical tip having a radius of 2.5 mm. It should be noted that although the integrated DIC-CBBM methodology [31] does not require the load data from the test machine for the calculation of fracture toughness properties, the load data of both ENF and SLB tests were recorded for subsequently justifying and validating the methodology, which will be addressed in Section 3.1.

For the fracture toughness characterisation testing at HR loading rates, all three types of tests were performed at an impact velocity of approximately 6 m/s by using modified SHPB systems, as illustrated in Figs. 3 and 4. For HR WDCB testing, the specimens were horizontally placed in an SHPB system consisting of a 2.7-m striker, a 2.5-m input bar

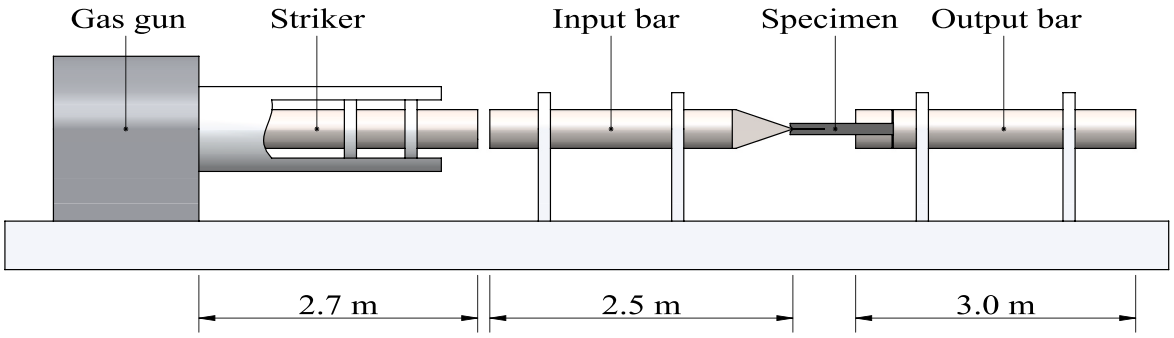

(a) SHPB setup for HR WDCB testing

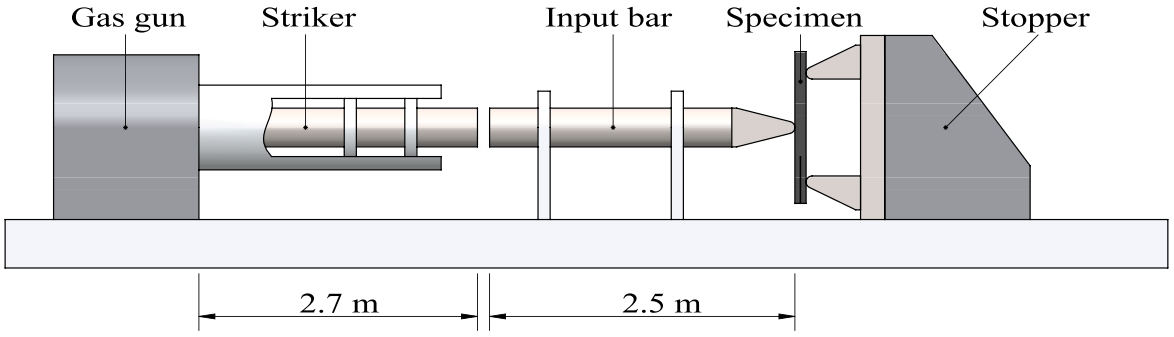

(b) SHPB setup for HR ENF testing

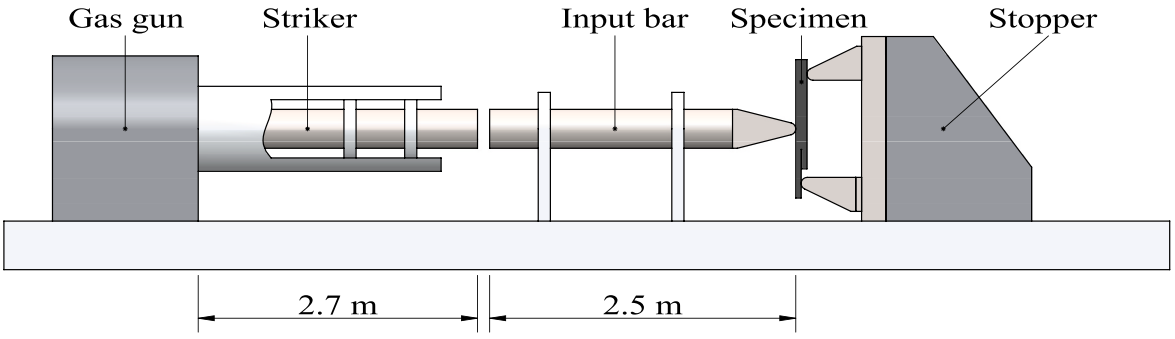

(c) SHPB setup for HR SLB testing

Fig. 3. SHPB setups for HR WDCB, ENF and SLB fracture toughness testing.

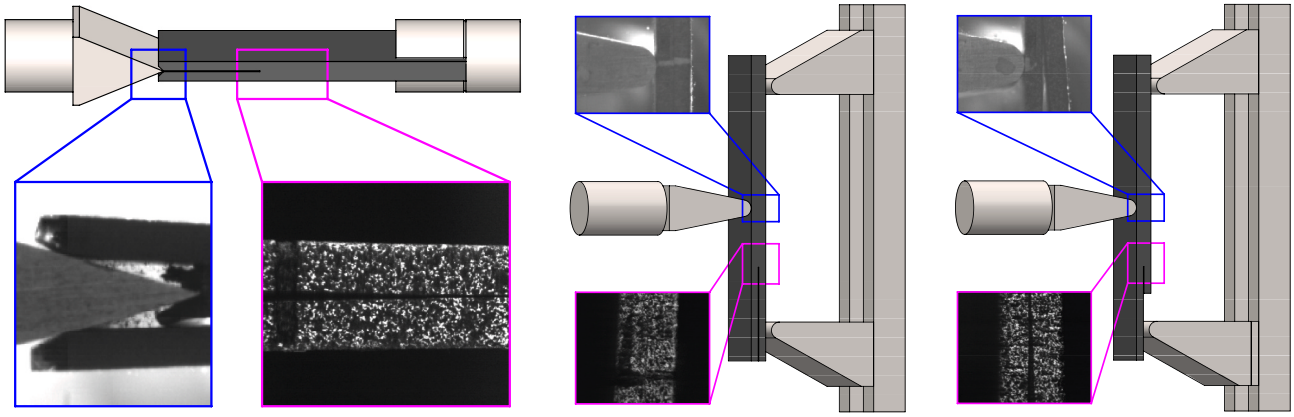

Fig. 4. WDCB, ENF and SLB setups for HR (6 m/s) fracture toughness testing.

screwed with a sharp-tip loading wedge, and a 3-m output bar connected with a notched cylindrical holder (Fig. 3a). During testing, two high-speed cameras (Fig. 4a) were utilised to record the HR test event. Specifically, the separation of each specimen at the free end was captured by a Photron camera at a frame rate of 100,000 fps and with a resolution of 320 × 192 pixels, while the propagation of the crack was monitored by a Specialised Imaging Kirana camera at a frame rate of 250,000 fps and with a resolution of 924 × 768 pixels. For HR ENF testing, tests were conducted on the SHPB system (Fig. 3b), which was modified from the HR WDCB SHPB system by using an input bar having a cylindrical-tip-based loading wedge and replacing the output bar with an in-house-made fixture to hold the specimen of testing vertically. The tip radii of the loading wedge and support blocks were the same and equal to 2.5 mm. During testing, the Photron camera was used to record the movement of the loading wedge at the same frame rate and resolution as HR WDCB testing, while the Kirana camera was employed to capture the propagation of the crack at a frame rate of 400,000 fps and with a resolution of 924 × 768 pixels (Fig. 4b). In terms of HR SLBtesting, the SHPB system, fixture and camera setups (Fig. 3c and 4c) were almost identical to those used in HR ENF testing, except that the height of one support block was augmented by two thin metal pads so that the specimens can be aligned perpendicularly to the impact direction. All the SHPB bars used have a diameter of 16 mm and were made from titanium alloy Ti–6Al–4V, with the elastic modulus, Poisson ratio and density being 114 GPa, 0.34 and 4.43 g/mm^3, respectively.

It should be noted that the SHPB systems were employed exclusively to generate HR loading conditions, and no attempt was made to apply the theory of SHPB to approximate the applied dynamic load. This was because the load calculated based on the strain gauge readings is believed to be not an accurate representation of the force acting on the specimen, owing to several inherent challenging factors of the experiments including I) a relatively large specimen size, II) profound geometric mismatch among the bars, loading wedge, specimen and support, and III) potential inertial effects of the specimen before and during crack propagation. Additionally, the load applied to the specimen has a small magnitude, and the accuracy of load measurement tends to be affected by the noise of the experiments. Given that the SHPB-theory-computed load is not sufficiently representative of the actual force, the integrated DIC-CBBM methodology was adopted to analytically calculate the applied dynamic load and HR fracture toughness property of each test based on the DIC data derived after performing DIC analysis of the recorded videos.

2.3. DIC data analysis

As demonstrated in the previous section, the primary raw data of the QS and HR experiments were test videos. To enable the application of the theories that will be described in Section 2.4 to analytically calculate the QS and HR fracture toughness properties of the material, the recorded videos of each test were analysed according to the DIC-based procedures previously established by the authors [31,34]. To calculate the Mode I fracture toughness, DIC analyses were performed on the WDCB test videos to extract two types of data, i.e., the opening displacement at the loading point (δ) and the crack length (a). The opening displacement was obtained by setting up a virtual extensometer (represented by line A_0B_0 in Fig. 5a) and measuring the extension of the virtual extensometer. In terms of the crack length of WDCB testing, it was determined by employing the DIC procedure illustrated in Fig. 5b. This approach is based on the use of a set of point pairs symmetrically placed on both sides of the expected crack path, where the first pair of points (A_1, B_1) is located at the initial crack tip. By tracking the displacements of these point pairs when performing a DIC analysis, the position of the current crack tip at a given frame time t can be roughly identified as in between the kth and (k+1)th point pairs if the following conditions are satisfied:

$$\Delta u_k(t) = \left|\Delta u_{A_k}(t) - \Delta u_{B_k}(t)\right| \geq \Delta u_{TH} \tag{1a}$$

$$\Delta u_{k+1}(t) = \left|\Delta u_{A_{k+1}}(t) - \Delta u_{B_{k+1}}(t)\right| \leq \Delta u_{TH} \tag{1b}$$

where Δu_{TH} is a displacement-based threshold for crack tip identification. Once the two point pairs are identified, the crack length can be computed by considering the x-coordinates of lines A_1B_1, A_kB_k and $A_{k+1}B_{k+1}$, as well as the displacement differences $\Delta u_k(t)$ and $\Delta u_{k+1}(t)$:

$$a(t) = a_0 + x_{A_k} - x_{A_1} + \frac{\Delta u_{TH} - \Delta u_k(t)}{\Delta u_{k+1}(t) - \Delta u_k(t)}\left(x_{A_{k+1}} - x_{A_k}\right) \tag{2}$$

To derive the Mode II fracture toughness properties, DIC analyses of the ENF test videos were conducted to generate two types of data, i.e., the displacement of the loading wedge (δ) and the crack length (a). The former was obtained directly when analysing the test video, while the latter was extracted following a DIC procedure modified from the one used for the WDCB case. In the DIC procedure for analysing ENF test videos, the y-displacements of pre-defined point pairs were used instead of their x-displacement components to identify the crack tip position and compute the crack length at time t. Given the high similarities between the ENF and SLB experiments, the same DIC procedures were employed

to analyse the SLB test videos to derive the displacement of the loading wedge (δ) and the crack length (a) for the sake of calculating the Mixed-mode I/II fracture toughness properties. Therefore, the equations for the crack tip identification and crack length calculation of ENF and SLB tests are the same and defined by:

$$\Delta v_{\mathrm{k}}(t) = \left|\Delta v_{\mathrm{A_k}}(t) - \Delta v_{\mathrm{B_k}}(t)\right| \geq \Delta v_{\mathrm{TH}} \tag{3a}$$

$$\Delta v_{\mathrm{k+1}}(t) = \left|\Delta v_{\mathrm{A_{k+1}}}(t) - \Delta v_{\mathrm{B_{k+1}}}(t)\right| \leq \Delta v_{\mathrm{TH}} \tag{3b}$$

$$a(t) = a_0 + x_{\mathrm{A_k}} - x_{\mathrm{A_1}} + \frac{\Delta v_{\mathrm{TH}} - \Delta v_{\mathrm{k}}(t)}{\Delta v_{\mathrm{k+1}}(t) - \Delta v_{\mathrm{k}}(t)}\left(x_{\mathrm{A_{k+1}}} - x_{\mathrm{A_k}}\right) \tag{3c}$$

2.4. Fracture toughness calculation

With the DIC-based results obtained by using the procedures described above, the fracture toughness properties of different delamination modes can be analytically computed using the compliance-based beam methods presented in Ref. [31]. For completeness and to demonstrate how the fracture toughness of a delamination mode can be derived entirely by using the DIC data (without the force data), the fundamental aspects of these methods are described in this section. For conciseness, the meaning of each variable in the mathematical equations that will be presented below has been summarised in the "Nomenclature" section and Fig. 1.

By employing the Timoshenko beam theory to deduce the elastic (bending and shear) energies stored in the specimen and applying the Castigliano second theorem, the compliance can be derived for Mode I (WDCB) [35], Mode II (ENF) [36] and Mixed-Mode I/II (SLB) [37] experiments, as follows:

$$\text{Mode I}: C = \frac{8a^3}{E_{\mathrm{f}}bh^3} + \frac{12a}{5G_{13}bh} \tag{4}$$

$$\text{Mode II}: C = \frac{3a^3 + 2L^3}{8E_{\mathrm{f}}bh^3} + \frac{3L}{10G_{13}bh} \tag{5}$$

$$\text{Mixed}-\text{mode}: C = \frac{28a^3 + L^3}{32E_{\mathrm{f}}bh^3} + \frac{3(a+L)}{20G_{13}bh} \tag{6}$$

where the flexural moduli for Mode I [35], Mode II [36] and Mixed-mode I/II [37] are defined by:

$$\text{Mode I}: E_{\mathrm{f}} = \frac{8(a_0+\Delta)^3}{bh^3}\left(C_0 - \frac{12(a_0+\Delta)}{5G_{13}bh}\right)^{-1} \tag{7}$$

$$\text{Mode II}: E_{\mathrm{f}} = \frac{3a_0^3 + 2L^3}{8bh^3}\left(C_0 - \frac{3L}{10G_{13}bh}\right)^{-1} \tag{8}$$

$$\text{Mixed}-\text{mode}: E_{\mathrm{f}} = \frac{28a_0^3 + L^3}{32bh^3}\left(C_0 - \frac{3(a_0+L)}{20G_{13}bh}\right)^{-1} \tag{9}$$

where the initial compliance C_0 of each mode was determined after conducting a simulation of the composite material under the corresponding mode of delamination, and the symbol Δ in Eq. (7) is a term accounting for the root rotation effect at the crack tip and given by Refs. [38,39]:

$$\Delta = h\sqrt{\frac{E_{\mathrm{f}}}{11G_{13}}\left[3 - 2\left(\frac{1.18\sqrt{E_{\mathrm{f}}E_3}}{G_{13} + 1.18\sqrt{E_{\mathrm{f}}E_3}}\right)^2\right]} \tag{10}$$

where it should be noted that Eqs. (7) and (10) do not yield an explicit expression for the E_{f} of Mode I, and the value of E_{f} can be numerically determined following an iterative solution procedure.

Based on the Irwin-Kies equation $\left(G_{\mathrm{c}} = \frac{F^2}{2b}\frac{dC}{da}\right)$ and the compliance formulae given above, the fracture toughness of each delamination mode can be defined by Refs. [31,36,37]:

$$G_{\mathrm{Ic}}(a,F) = \frac{12a^2F^2}{E_{\mathrm{f}}b^2h^3} + \frac{6F^2}{5G_{13}b^2h} \tag{11}$$

$$G_{\mathrm{IIc}}(a_{\mathrm{e}},F) = \frac{9a_{\mathrm{e}}^2F^2}{16E_{\mathrm{f}}b^2h^3} \tag{12}$$

$$G_{\mathrm{I/IIc}}(a,F) = \frac{21a^2F^2}{16E_{\mathrm{f}}b^2h^3} + \frac{3F^2}{40G_{13}b^2h} \tag{13}$$

where a_{e} in Eq. (12) is the crack length corrected by including the FPZ

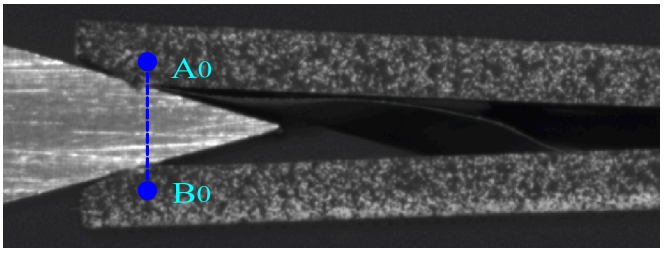

(a) Opening displacement at the loading point

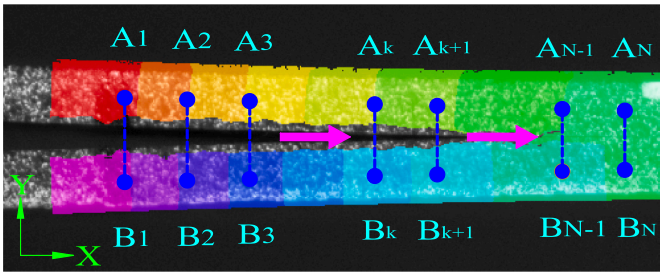

(b) DIC-based extraction of crack length

Fig. 5. DIC-based extraction of opening displacement and crack length for WDCB testing.

effect and can be defined by Ref. [36]:

$$a_e = \sqrt[3]{\frac{C_c}{C_{0c}}a_0^3 + \frac{2}{3}\left(\frac{C_c}{C_{0c}} - 1\right)L^3} \tag{14}$$

where C_c and C_{0c} are two intermediate variables given by:

$$C_c = C - \frac{3L}{10G_{13}bh}, C_{0c} = C_0 - \frac{3L}{10G_{13}bh} \tag{15}$$

To bypass the measurement of force data in the fracture toughness characterisation experiments, the forces in Eqs. (11)–(13) can be replaced by considering the relationship among the applied load (F), the displacement (δ) and the compliance (C) of the beam:

$$F = \delta / C \tag{16}$$

Based on Eqs. (4)–(6) and by replacing the forces in Eqs. (11)–(13) with Eq. (16), the Mode I, Mode II and Mixed-mode I/II fracture toughness properties can be completely expressed as functions of the DIC-based data described in Section 2.3, i.e., the total crack length (a), the opening displacement or beam deflection (δ). This avoids the need for measuring the force data directly. Here, it should be noted that the equations above were originally developed for QS loading conditions, and their applicability to HR loading scenarios needs to be justified and will be addressed in Section 3.1. The material properties used for calculating the fracture toughness properties were extracted from the Hexcel data sheet [33]: $E_1 = 182$ GPa, $E_3 = 9.0$ GPa and $G_{13} = 4.5$ GPa.

3. Results & discussion

3.1. Validation of experimental methodology

Since the integrated DIC-CBBM methodology was developed originally for adhesively bonded structures, the use of this methodology to study the fracture behaviour of CFRP composites needs to be justified. The applicability of this methodology for QS loading conditions was directly evaluated by comparing the load-displacement response obtained using the DIC-CBBM method and that measured based on the load cell. Fig. 6 illustrates that the load-deflection curves derived using the two different approaches match perfectly with each other, validating the integrated DIC-CBBM methodology for both ENF and SLB testing at QS loading conditions. Here, it should be noted that the validation of the proposed approach for QS WDCB testing cannot be performed due to the difficulty of measuring the opening force in a WDCB test. However, given that the integrated DIC-CBBM methodology is valid for QS Mixed-mode I/II (SLB) testing, which contains a large portion of Mode I delamination, it can be assumed that this methodology is also applicable to QS Mode I (WDCB) testing in the present research.

As described in Ref. [31], the principle for evaluating the validity of the proposed methodology for calculating the fracture toughness of an HR test is to examine whether the HR test exhibits a pseudo-QS response, which is characterised by the HR test achieving force equilibrium and the specimen undergoing a deformation pattern similar to that in a QS test. For force equilibrium, it can be determined by comparing the reference time (t_R - test duration) against the characteristic time (t_T - the duration of the elastic wave in the loading pin travelling through the whole specimen thickness) and the support reaction time (t_C - twice the duration of the elastic wave travelling from the impact location to supports) [40]. Table 1 details the different times of the three types of HR delamination tests. It is evident that both the characteristic time and support reaction time were significantly smaller than the reference time, suggesting that dynamic force equilibrium was achieved in these HR tests. Fig. 7 shows the deformation histories of typical QS and HR WDCB tests. Here, a good match between the QS and HR deformation patterns implies a pseudo-QS response in HR delamination tests. Based on the above, it is assumed that the integrated DIC-CBBM methodology is also valid for the HR delamination tests of the present work.

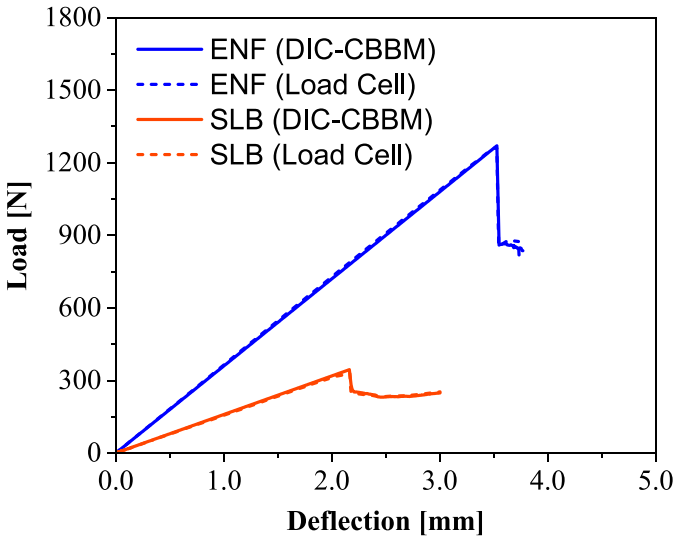

Fig. 6. Validation of the integrated DIC-CBBM methodology for computing QS (1 mm/min) fracture toughness properties via a comparison of typical load-deflection curves obtained by using the Zwick load cell and the DIC-CBBM method.

Table 1
Summary of the reference time, characteristic time and support reaction time of the three modes of HR (6 m/s) delamination tests.

Mode	t_R [μs]	t_T [μs]	t_C [μs]
HR WDCB	280	0.8	56
HR ENF	200	0.8	26
HR SLB	220	0.8	26

It is worth noting that, when using the DIC-CBBM methodology for new dynamic delamination tests, the validation process above always needs to be performed. Also, this methodology can be applied only when 1) the characteristic time and support time of the dynamic test are way

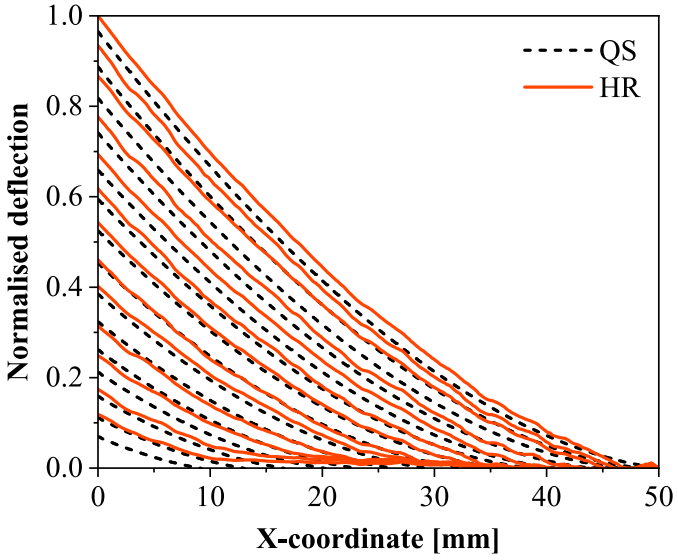

Fig. 7. Validation of the integrated DIC-CBBM methodology for computing HR fracture toughness properties via a comparison of the deflections of typical WDCB tests at QS (1 mm/min) and HR (6 m/s) conditions.

smaller than the reference time and 2) the corresponding specimen shows a pseudo-QS deformation pattern.

3.2. Interlaminar delamination behaviour

By employing the DIC analysis procedure described in Section 2.3 and the CBBM-based approach in Section 2.4, the load-displacement response of each delamination test can be obtained. Fig. 8a shows the load-displacement curves of the WDCB tests. It is evident that both the QS and HR WDCB results have good repeatability, with the QS and HR loads peaking at 88.29 N and 103.86 N, respectively. In terms of the ENF results (Fig. 8b), all load-deflection curves coincided at the initial elastic region. Although there was some scatter in the results, the maximum loads of the HR ENF tests were higher than those of the QS ENF tests,

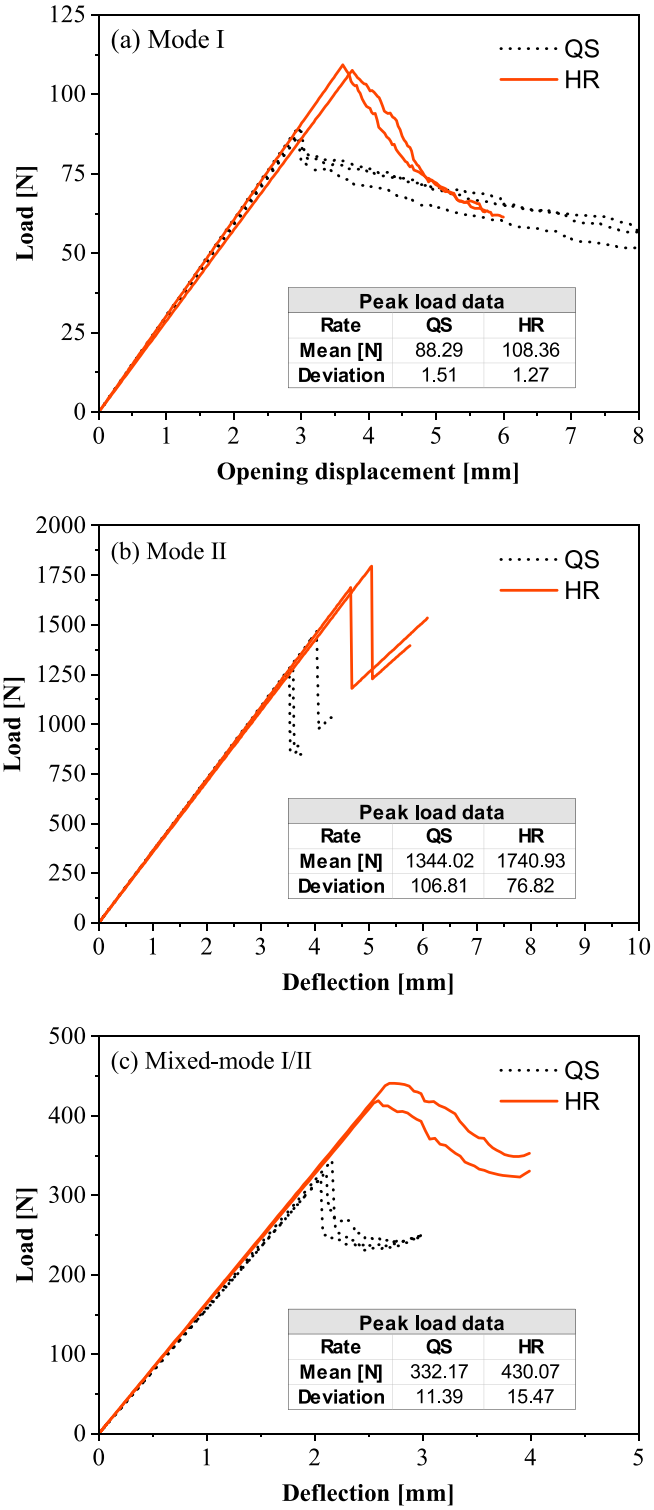

Fig. 8. Load-displacement response of a) Mode I: WDCB, b) Mode II: ENF, and c) Mixed-mode I/II: SLB tests at QS (1 mm/min) and HR (6 m/s) conditions.

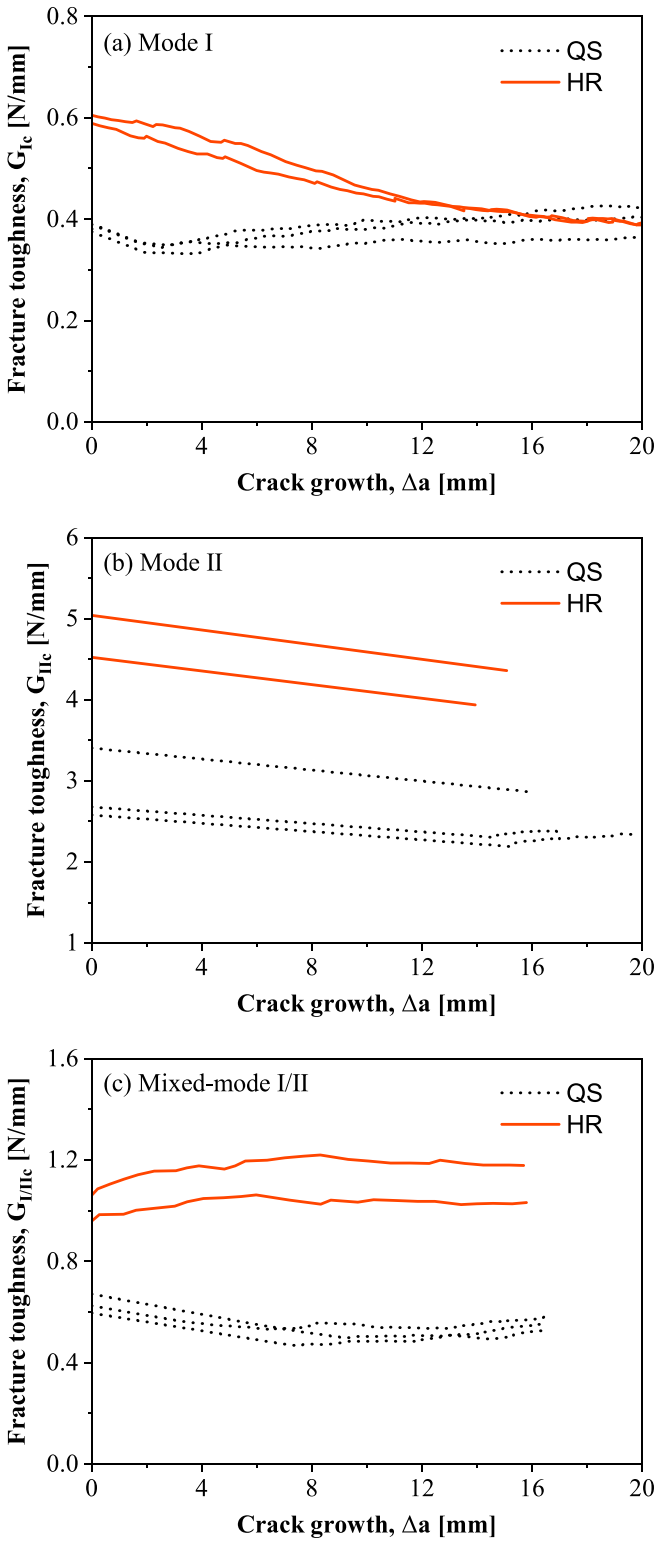

Fig. 9. Fracture behaviour of a) Mode I: WDCB, b) Mode II: ENF, and c) Mixed-mode I/II: SLB tests at QS (1 mm/min) and HR (6 m/s) loadings.

with an average peak value of 1740.93 N for the HR condition and 1344.02 N for the QS rate. The load-deflection results of the SLB tests are plotted in Fig. 8c. Despite that one of the QS tests exhibited a lower stiffness, the QS tests again demonstrated lower peaks than the HR tests, and the corresponding average values of the QS and HR peak loads were 332.17 N and 430.07 N, respectively. The load-displacement results in Fig. 8 suggest that, compared to QS rates, a higher load was needed to trigger delamination at HR conditions. This indicates that the CFRP material of investigation has at least a rate-dependent behaviour at the point of delamination initiation.

To quantify the delamination behaviour of the composite, the fracture toughness of each test was calculated using Eqs. (11)–(13). The results of the WDCB tests (Mode I delamination) are illustrated in Fig. 9a, where each curve represents the variation of the fracture

Table 2
Mean values and standard deviations for the initiation fracture toughness properties of Mode I (WDCB), Mode II (ENF) and Mixed-mode I/II (SLB) delamination.

Loading rate	WDCB	ENF	SLB
QS G_c [N/mm]	0.382 ± 0.007	2.886 ± 0.450	0.630 ± 0.038
HR G_c [N/mm]	0.597 ± 0.011	4.780 ± 0.365	1.009 ± 0.072
HR G_c/QS G_c	1.56	1.66	1.60

toughness against the crack growth. It can be seen that, compared to the HR cases, the QS WDCB tests had higher fracture toughness from the onset of delamination to a crack growth of approximately 15 mm. The average QS and HR fracture toughness values at crack initiation are about 0.38 N/mm and 0.60 N/mm, respectively. It is worth noting that the QS WDCB tests exhibited mild fluctuations of the fracture toughness against the crack growth. However, the curves of the HR WDCB tests showed monotonic decreasing trends, with the fracture toughness gradually dropping to a level similar to the QS results at a crack growth of approximately 18 mm. The fracture toughness results of the ENF tests (Mode II delamination) are presented in Fig. 9b. Similar to the corresponding load-deflection curves (Fig. 8b), there was some scatter in the computed fracture toughness. However, there is no doubt that the HR tests showed considerably higher resistance to delamination in the full range of the crack growth, and the average QS and HR toughness values at delamination initiation are about 2.89 N/mm and 4.78 N/mm, respectively. Here, it should be noted that the linear decreasing trends of the curves were found to be a result of unstable crack propagation. In terms of the SLB tests (Mixed-mode delamination), the corresponding results are given in Fig. 9c. Again, the HR toughness curves are higher than the QS cases, with the average values at fracture initiation being 1.01 N/mm and 0.63 N/mm, respectively. As indicated in the QS curves, unstable crack propagation also occurred in the QS SLB tests.

It should be noted that the presence of unstable crack propagation in some tests somehow affected the fracture toughness results at the stage of crack progression. However, it is evident that the HR fracture toughness curves are higher than the QS counterparts, which suggests that the interlaminar delamination behaviour of the composite was positively dependent on the loading rate, not only at the crack initiation point but also at the crack propagation stage. For the reader's convenience, the initiation fracture toughness properties of the composite subjected to the three modes of delamination are summarised in Table 2. As quantified in this table, the HR fracture toughness properties of Mode I, Mode II and Mixed-mode I/II accounted for 1.56, 1.66 and 1.60 times the QS properties, respectively.

To facilitate numerical modelling, both the Benzeggagh-Kenane (BK) criterion (Eq. (17)) and the power law (PL) criterion (Eq. (18)) were employed to fit against the characterised toughness properties by using the least squares method. The best-fitted failure envelopes based on the two criteria are displayed in Fig. 10, with the fitted powers being $\eta = 2.72$ and $\alpha = 1.27$, respectively. This will enable design engineers to interpolate the fracture toughness properties of the material at the loading rates of interest.

$$\text{BK}: G_c = G_{Ic} + (G_{IIc} - G_{Ic})(G_{II}/G_T)^{\eta} \tag{17}$$

$$\text{PL}: G_c = \left[\frac{1}{G_{Ic}^{\alpha}}\left(1 - \frac{G_{II}}{G_T}\right)^{\alpha} + \frac{1}{G_{IIc}^{\alpha}}\left(\frac{G_{II}}{G_T}\right)^{\alpha}\right]^{-\frac{1}{\alpha}} \tag{18}$$

where $G_T = G_I + G_{II}$.

3.3. Fractographic analysis

Further to the QS and HR delamination tests, a detailed fracture analysis based on optical 3D metrology and SEM was conducted to investigate the failure characteristics of tested specimens and thus establish the relationship between the rate-dependent delamination behaviour of the CFRP material and the underlying failure mechanisms at different test conditions. For optical 3D metrology, a highly flexible 3D optical measurement device (Alicona InfiniteFocus) was employed to measure the surface profiles of tested specimens near their initial crack tips. The optical measurement was conducted at a resolution of approximately 150,000 data points per square millimetre, and the results are shown in Fig. 11. Here, the 3D surface profiles were directly measured using the Alicona device, while the 2D curves represent the average profile height of all measured cross-sections perpendicular to the direction of crack propagation. The optical data clearly illustrates that, for all three delamination modes, the QS specimens manifested rougher fracture surfaces compared to the HR specimens. It should be noted that, with the same failure mechanisms, a rougher fracture surface is generally associated with a higher degree of energy dissipation and thus an increased fracture toughness. The finding of the QS tests having rougher fracture surfaces is seemingly contradictory to the results shown in Section 3.2: the QS tests exhibited lower fracture toughness values.

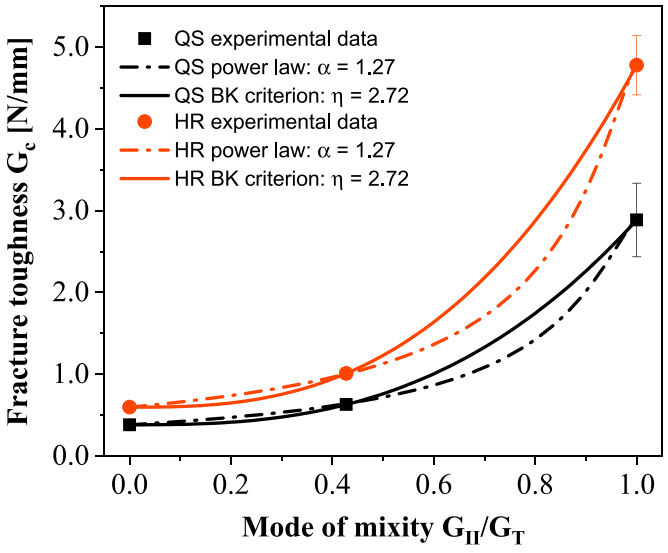

Fig. 10. Summary of the rate-dependent interlaminar fracture behaviour of the CFRP composites.

To understand why the QS tests manifested rougher fracture surfaces but yet had lower fracture toughness properties, a post-mortem SEM analysis of the fractured sample's interfaces was conducted by using a Zeiss SEM machine. Fig. 12 shows the SEM micrographs of the WDCB specimens tested at QS and HR conditions, respectively. As can be seen clearly in the figure, the QS WDCB specimen experienced a large amount of fibre-matrix interface debonding and plucking of toughening particles, resulting in a considerably rough fracture surface. In contrast, the predominant failure mode of the HR WDCB specimen was matrix cracking, exhibiting a smoother fracture morphology. The transition of the delamination failure (from a combination of fibre-matrix debonding and matrix cracking in the QS condition to primarily matrix failure in the HR scenario) was also observed by Riezzo et al. [12] in the delamination testing of IM7/M91. Similarly, they found that the HR fracture toughness properties were significantly higher than the QS values. According to Bradley's study of three CFRP composites (T6T145/F185, C6000/HX206, C6000/HX210) [41], the delamination toughness properties of the pure epoxy resins were much higher than those of the corresponding composites. In other words, for the same area of delamination the amount of energy dissipated in the matrix cracking mode of a composite material can be higher than that dissipated in the fibre-matrix debonding mode. Therefore, it can be argued that the presence of more evident fibre-matrix debonding in the QS WDCB tests accounts for the

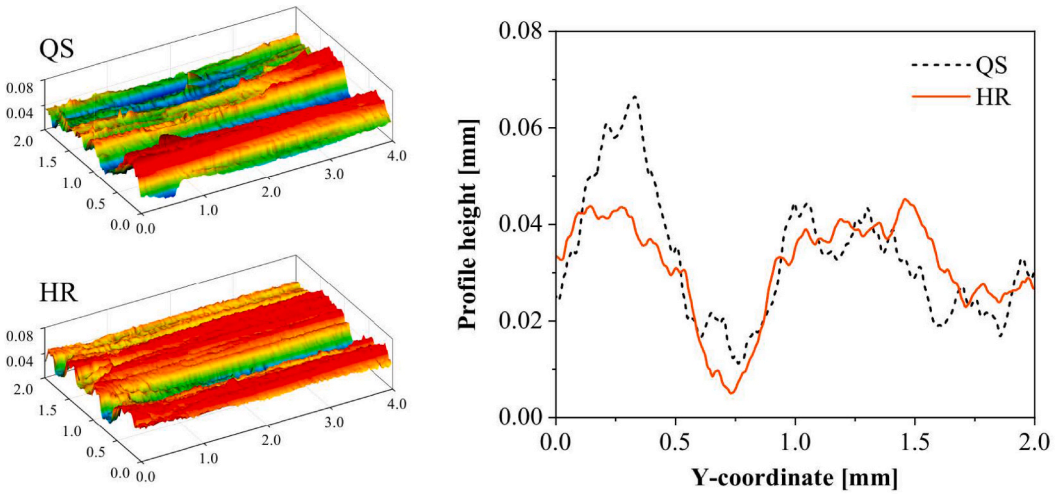

(a) Typical fracture surface profiles of Mode I: WDCB tests

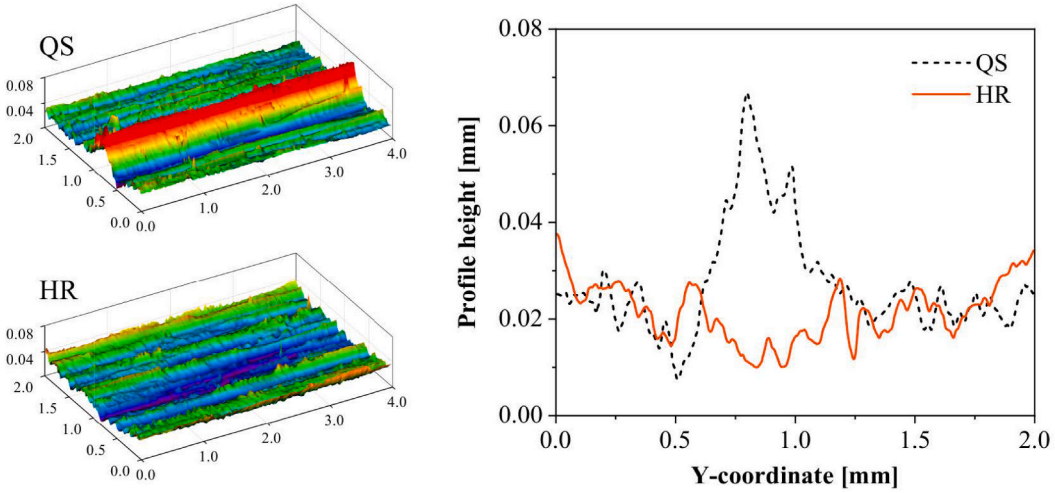

(b) Typical fracture surface profiles of Mode II: ENF tests

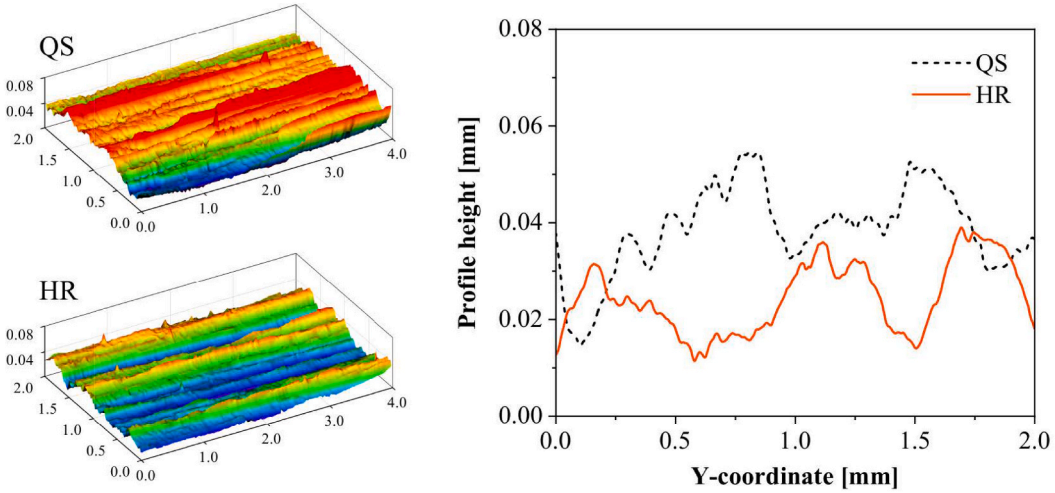

(c) Typical fracture surface profiles of Mixed-mode I/II: SLB tests

Fig. 11. Typical fracture surface profiles of a) Mode I: WDCB, b) Mode II: ENF, and c) Mixed-mode I/II: SLB tests at QS (1 mm/min) and HR (6 m/s) conditions (Direction of crack propagation: rightward).

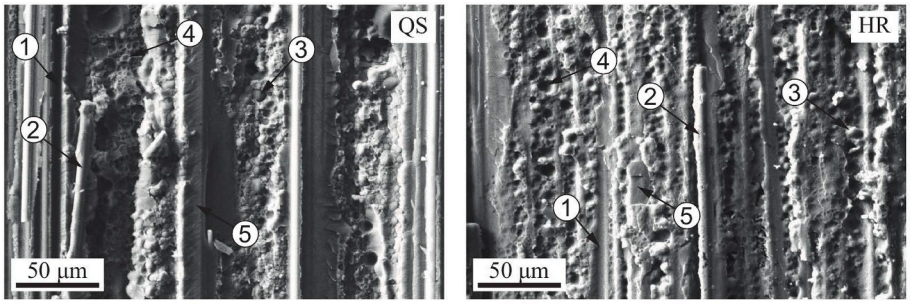

① Fibre tracks: fibre/matrix debonding, ② Broken fibres, ③ Spherical toughening particles
④ Toughening particles plucked from parent matrix, ⑤ Cohesive matrix delamination

Fig. 12. SEM micrographs of WDCB specimens fractured at QS (1 mm/min) and HR (6 m/s) conditions (Direction of crack propagation: downward).

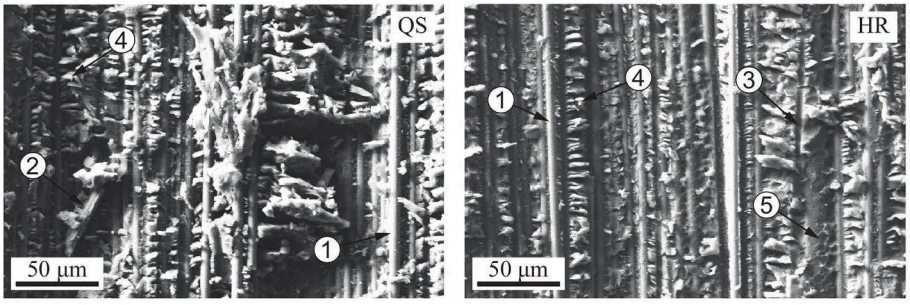

① Fully exposed fibres, ② Broken fibres, ③ Fibre tracks: fibre/matrix debonding, ④ Cusps
⑤ Toughening particles plucked from parent resin (fracture surfaces partially smeared)

Fig. 13. SEM micrographs of ENF specimens fractured at QS (1 mm/min) and HR (6 m/s) conditions (Direction of crack propagation: downward).

QS WDCB specimens having rougher fracture surfaces but lower fracture toughness values, compared to the HR WDCB counterparts.

The SEM micrographs of the QS and HR ENF specimens are shown in Fig. 13. Although it is somewhat difficult to interpret the fracture morphologies (affected by the friction and relative motion between the lower and upper fracture faces) [42], the predominant failure mechanisms of both the QS and HR ENF specimens were a combination of fibre-matrix interface debonding and prevalent shear failure in the form of cusps. Also, the fracture surface of the HR ENF specimen is smoother compared to that of the QS ENF specimen, suggesting a reduced possibility of the crack propagating through fibre-matrix interfaces and thus increased resistance to fracture (Fig. 9b). The SEM results of the QS and HR SLB tests are presented in Fig. 14. Unsurprisingly, these SEM micrographs are similar to those of the WDCB cases (Fig. 12), which is because the SLB tests underwent a considerable portion of Mode I delamination. Again, fibre-matrix debonding was more prevalent in the QS specimen, which implies that less energy was needed to delaminate the QS SLB specimen.

The above SEM analysis explains the seemingly contradictory finding obtained by the 3D optical metrology. Arguably, it was the occurrence of more prevalent fibre-matrix debonding in the QS tests that resulted in rougher fracture surfaces but lower fracture toughness values. However, one may question why in the HR delamination tests fibre-matrix debonding, which required less energy, was much less common than matrix cracking. It is postulated that such a phenomenon was a result of a notable difference in the loading rates of the QS and HR tests. In the QS tests, the displacement rate was so small (1 mm/min) that the crack was allowed to propagate at a low velocity (approximately in the order of 1 mm/s). As a result, the damage near the crack tip was more diffused, leading to the migration of cracks from the inter-ply region to the fibre-

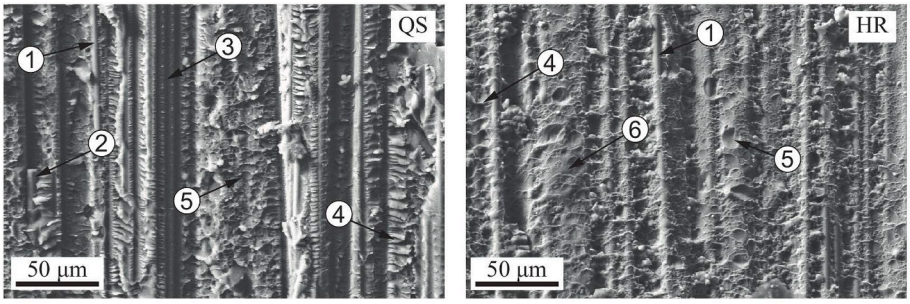

① Fully exposed fibres, ② Broken fibres, ③ Fibre tracks: fibre/matrix debonding, ④ Cusps
⑤ Toughening particles plucked from parent resin (no smearing), ⑥ Smeared resin failure

Fig. 14. SEM micrographs of SLB specimens fractured at QS (1 mm/min) and HR (6 m/s) conditions (Direction of crack propagation: downward).

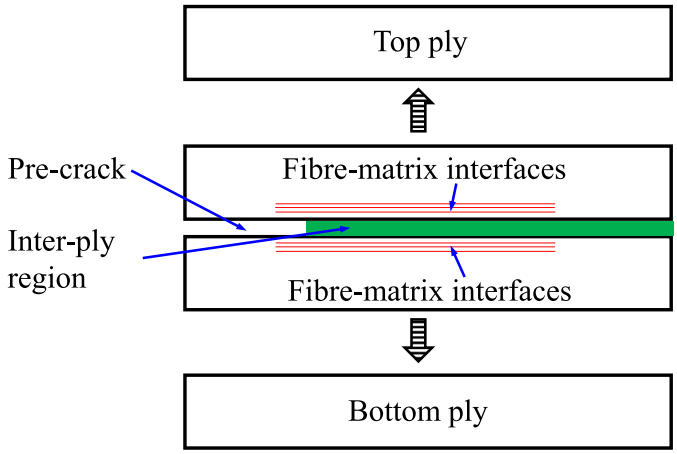

Fig. 15. Schematic illustration of the inter-ply region and adjacent fibre-matrix interfaces of a typical specimen for interlaminar delamination testing.

matrix interfaces of the plies adjacent to the inter-ply region, as schematically illustrated in Fig. 15. By contrast, the displacement rate of the HR tests was so high (6 m/s) that the crack was forced to advance at a massively higher velocity (in the order of 100 m/s). At such a high propagation velocity, the damage near the crack tip was more confined within the inter-ply region, limiting the migration of cracks into the adjacent plies. Therefore, despite requiring less energy to be triggered, fibre-matrix debonding tended to become a secondary failure mode in the HR tests and was not as common as in the QS tests. Based on the above analysis, it is established that the positively rate-dependent fracture behaviour of the CFRP material was associated with the transition of the predominant failure mechanism, featuring a decrease of fibre-matrix interface debonding and an increase of matrix cracking when the loading rate was increased.

4. Conclusions

This work systematically investigated the rate-dependent interlaminar delamination behaviour of a commercial CFRP material by conducting Mode I (WDCB), Mode II (ENF) and Mixed-mode I/II (SLB) delamination tests at both QS and HR loading conditions, which were performed on a standard screw-driven test machine and in-house SHPB systems, respectively. To minimise potential discrepancies associated with different operators and methodologies, all three types of delamination tests were undertaken within a single experimental programme, and an integrated DIC-CBBM methodology was employed for the data reduction and analysis of all test results. Following the experiments, a detailed fractographic analysis was carried out to correlate the rate-dependent delamination behaviour and the underlying failure mechanisms. The following conclusions can be drawn from the present research.

- The integrated DIC-CBBM methodology was proven to be valid for the data reduction and analysis of the delamination tests in the present work.
- The interlaminar delamination behaviour of the investigated CFRP material was found to be positively dependent on the loading rate, with the Mode I, Mode II, and Mixed-mode fracture toughness properties (at the onset of delamination) under the HR loading rate being 1.56, 1.66 and 1.60 times the corresponding values at the QS loading condition, respectively.
- The results obtained from the 3D optical metrology revealed that all three modes of delamination at the QS loading condition tended to create rougher fracture interfaces compared to their HR counterparts.
- The SEM images highlighted the predominant failure mechanisms transiting from a combination of fibre-matrix debonding and matrix cracking in the QS tests to primarily matrix failure in the HR tests. The transition of the predominant failure mechanisms at QS and HR loading conditions confirms the positively rate-dependent delamination behaviour of the CFRP material.

Author statement

I confirm that the work described has not been published previously (except in the form of an abstract, a published lecture or academic thesis), that it is not under consideration for publication elsewhere, that its publication is approved by all authors and tacitly or explicitly by the responsible authorities where the work was carried out, and that, if accepted, it will not be published elsewhere in the same form, in English or in any other language, including electronically without the written consent of the copyright-holder.

Declaration of competing interest

The authors declare that they have no known competing financial interests or personal relationships that could have appeared to influence the work reported in this paper.

Data availability

The authors are unable or have chosen not to specify which data has been used.

Acknowledgements

This work was supported by the DELICE project (Design of Engineered Lightweight Innovative Casings for Engines) funded by Innovate UK under Grant No. 113106. The authors would like to acknowledge Rolls-Royce plc for providing the material, Dr Lorenzo Mencattelli at Imperial College London for curing the laminated plate, and Mr Stuart Carter at the University of Oxford for machining the specimens.

References

[1] Chawla KK. Composite materials: science and engineering. third ed. Springer-Verlag New York; 2012. https://doi.org/10.1007/978-0-387-74365-3.
[2] Smiley AJ, Pipes RB. Rate effects on mode I interlaminar fracture toughness in composite materials. J Compos Mater 1987;21. https://doi.org/10.1177/002199838702100706.
[3] Gillespie JW, Carlsson LA, Smiley AJ. Rate-dependent mode I interlaminar crack growth mechanisms in graphite/epoxy and graphite/PEEK. Compos Sci Technol 1987;28. https://doi.org/10.1016/0266-3538(87)90058-3.
[4] Yaniv G, Daniel IM. Height-tapered double cantilever beam specimen for study of rate effects on fracture toughness of composites. ASTM Spec. Tech. Publ.; 1988. https://doi.org/10.1520/stp26139s.
[5] Blackman BRK, Dear JP, Kinloch AJ, Macgillivray H, Wang Y, Williams JG, et al. The failure of fibre composites and adhesively bonded fibre composites under high rates of test - Part I Mode I loading-experimental studies. J Mater Sci 1995;30. https://doi.org/10.1007/BF01151502.
[6] You H, Yum YJ. Loading rate effect on mode I interlaminar fracture of carbon/epoxy composite. J Reinforc Plast Compos 1997;16. https://doi.org/10.1177/073168449701600604.
[7] Kusaka T, Hojo M, Mai YW, Kurokawa T, Nojima T, Ochiai S. Rate dependence of mode I fracture behaviour in carbon-fibre/epoxy composite laminates. Compos Sci Technol 1998;58. https://doi.org/10.1016/S0266-3538(97)00176-0.
[8] Wu XF, Dzenis YA. Determination of dynamic delamination toughness of a graphite-fiber/epoxy composite using hopkinson pressure bar. Polym Compos 2005;26. https://doi.org/10.1002/pc.20093.
[9] Hug G, Thévenet P, Fitoussi J, Baptiste D. Effect of the loading rate on mode I interlaminar fracture toughness of laminated composites. Eng Fract Mech 2006;73. https://doi.org/10.1016/j.engfracmech.2006.05.019.
[10] Zabala H, Aretxabaleta L, Castillo G, Aurrekoetxea J. Loading rate dependency on mode I interlaminar fracture toughness of unidirectional and woven carbon fibre epoxy composites. Compos Struct 2015;121. https://doi.org/10.1016/j.compstruct.2014.11.001.
[11] Thorsson SI, Waas AM, Schaefer J, Justusson B, Liguore S. Effects of elevated loading rates on mode I fracture of composite laminates using a modified wedge-

insert fracture method. Compos Sci Technol 2018;156. https://doi.org/10.1016/j.compscitech.2017.12.018.
[12] Riezzo MA, Simmons M, Russell B, Sket F, Martínez V, González C. Dynamic characterisation of interlaminar fracture toughness in carbon fibre epoxy composite laminates. Composer Part A Appl Sci Manuf 2019;126. https://doi.org/10.1016/j.compositesa.2019.105597.
[13] Isakov M, May M, Hahn P, Paul H, Nishi M. Fracture toughness measurement without force data – application to high rate DCB on CFRP. Composer Part A Appl Sci Manuf 2019;119. https://doi.org/10.1016/j.compositesa.2019.01.030.
[14] Smiley AJ, Pipes RB. Rate sensitivity of mode II interlaminar fracture toughness in graphite/epoxy and graphite/PEEK composite materials. Compos Sci Technol 1987;29. https://doi.org/10.1016/0266-3538(87)90033-9.
[15] Maikuma H, Gillespie JW, Wilkins DJ. Mode II interlaminar fracture of the center notch flexural specimen under impact loading. J Compos Mater 1990;24. https://doi.org/10.1177/002199839002400201.
[16] Kageyama K, Kimpara I. Delamination failures in polymer composites. Mater Sci Eng, A 1991;143. https://doi.org/10.1016/0921-5093(91)90736-7.
[17] Kusaka T, Yamauchi Y, Kurokawa T. Effects of strain rate on mode II interlaminar fracture toughness in carbon-fibre/epoxy laminated composites. J Phys IV JP 1994;4. https://doi.org/10.1051/jp4:19948102.
[18] Blackman BRK, Dear JP, Kinloch AJ, MacGillivray H, Wang Y, Williams JG, et al. The failure of fibre composites and adhesively bonded fibre composites under high rates of test: Part III mixed-mode I/II and mode II loadings. J Mater Sci 1996;31. https://doi.org/10.1007/BF00366342.
[19] Tsai JL, Guo C, Sun CT. Dynamic delamination fracture toughness in unidirectional polymeric composites. Compos Sci Technol 2001;61. https://doi.org/10.1016/S0266-3538(00)00197-4.
[20] Zabala H, Aretxabaleta L, Castillo G, Aurrekoetxea J. Dynamic 4 ENF test for a strain rate dependent mode II interlaminar fracture toughness characterization of unidirectional carbon fibre epoxy composites. Polym Test 2016;55. https://doi.org/10.1016/j.polymertesting.2016.09.001.
[21] Machado JJM, Marques EAS, Campilho RDSG, da Silva LFM. Mode II fracture toughness of CFRP as a function of temperature and strain rate. Compos B Eng 2017;114. https://doi.org/10.1016/j.compositesb.2017.02.013.
[22] Yasaee M, Mohamed G, Pellegrino A, Petrinic N, Hallett SR. Strain rate dependence of mode II delamination resistance in through thickness reinforced laminated composites. Int J Impact Eng 2017;107. https://doi.org/10.1016/j.ijimpeng.2017.05.003.
[23] Kusaka T, Horikawa N, Masuda M. Low-velocity impact fracture behaviour of impact-resistant polymer matrix composite laminates under mixed mode loading. J Phys IV JP 2000;10. https://doi.org/10.1051/jp4:2000953.
[24] Oshima S, Ishida H, Kusaka T, Takeda T. Experimental characterization of dynamic crack growth behavior in CFRP adhesive interface. Adv Compos Mater 2018;27. https://doi.org/10.1080/09243046.2017.1401336.
[25] Jacob GC, Starbuck JM, Fellers JF, Simunovic S, Boeman RG. The effect of loading rate on the fracture toughness of fiber reinforced polymer composites. J Appl Polym Sci 2005;96. https://doi.org/10.1002/app.21535.
[26] May M. Measuring the rate-dependent mode I fracture toughness of composites - a review. Composer Part A Appl Sci Manuf 2016;81. https://doi.org/10.1016/j.compositesa.2015.10.033.
[27] May M, Channammagari H, Hahn P. High-rate mode II fracture toughness testing of polymer matrix composites – a review. Composer Part A Appl Sci Manuf 2020;137. https://doi.org/10.1016/j.compositesa.2020.106019.
[28] Liu H, Nie H, Zhang C, Li Y. Loading rate dependency of Mode I interlaminar fracture toughness for unidirectional composite laminates. Compos Sci Technol 2018;167. https://doi.org/10.1016/j.compscitech.2018.07.040.
[29] Liu H, Meng X, Zhang H, Nie H, Zhang C, Li Y. The dynamic crack propagation behavior of mode I interlaminar crack in unidirectional carbon/epoxy composites. Eng Fract Mech 2019;215. https://doi.org/10.1016/j.engfracmech.2019.05.004.
[30] Ponnusami SA, Cui H, Erice B, Lißner M, Pathan M, Petrinic N. An integrated inverse numerical–experimental approach to determine the dynamic Mode-I interlaminar fracture toughness of fibre composites. Compos Struct 2022;293. https://doi.org/10.1016/j.compstruct.2022.115734.
[31] Lißner M, Alabort E, Erice B, Cui H, Blackman BRK, Petrinic N. On the dynamic response of adhesively bonded structures. Int J Impact Eng 2020;138. https://doi.org/10.1016/j.ijimpeng.2019.103479.
[32] Lißner M, Erice B, Alabort E, Thomson D, Cui H, Kaboglu C, et al. Multi-material adhesively bonded structures: characterisation and modelling of their rate-dependent performance. Compos B Eng 2020;195. https://doi.org/10.1016/j.compositesb.2020.108077.
[33] Corporation Hexcel. HexPly M56: 180°C (350°F) out-of-autoclave curing matrix [product data sheet]. https://www.hexcel.com/user_area/content_media/raw/HexPly_M56_global_DataSheet.pdf; 2021. August 8, 2021.
[34] Chen Y, Liu H, Liu K, Lißner M, Xu Z, Pashley D, et al. Application of digital image correlation for crack length measurement in WDCB-based mode I fracture toughness testing of composites. In: Kang J, McKeighan PC, Dahlberg G, Kemmerer B, editors. Eval. Exist. New sens. Technol. Fatigue, fract. Mech. Test. West Conshohocken, PA: ASTM International; 2022. p. 67–82.
[35] Fernández MV, de Moura MFSF, da Silva LFM, Marques AT. Composite bonded joints under mode I fatigue loading. Int J Adhesion Adhes 2011;31:280–5. https://doi.org/10.1016/j.ijadhadh.2010.10.003.
[36] de Moura MFSF, Silva MAL, de Morais AB, Morais JJL. Equivalent crack based mode II fracture characterization of wood. Eng Fract Mech 2006;73. https://doi.org/10.1016/j.engfracmech.2006.01.004.
[37] Oliveira JMQ, de Moura MFSF, Morais JJL. Application of the end loaded split and single-leg bending tests to the mixed-mode fracture characterization of wood. Holzforschung 2009;63. https://doi.org/10.1515/HF.2009.088.
[38] de Moura MFSF, Morais JJL, Dourado N. A new data reduction scheme for mode I wood fracture characterization using the double cantilever beam test. Eng Fract Mech 2008;75. https://doi.org/10.1016/j.engfracmech.2008.02.006.
[39] Hashemi S, James AJ, Williams JM. The analysis of interlaminar fracture in uniaxial fibre-polymer composites. Proc R Soc London A Math Phys Sci 1990;427. https://doi.org/10.1098/rspa.1990.0007.
[40] Delvare F, Hanus JL, Bailly P. A non-equilibrium approach to processing Hopkinson Bar bending test data: application to quasi-brittle materials. Int J Impact Eng 2010;37. https://doi.org/10.1016/j.ijimpeng.2010.07.001.
[41] Bradley WL. Relationship of matrix toughness to interlaminar fracture toughness. Compos Mater 1989;6. https://doi.org/10.1016/B978-0-444-87286-9.50009-7.
[42] Greenhalgh ES. Failure analysis and fractography of polymer composites. 2009. https://doi.org/10.1533/9781845696818.